Investigation of Standoff Explosives Detection via Photothermal/Photoacoustic Interferometry

Pak S. Cho[*a], Robert M. Jones[b], Timothy Shuman[†b], Daniel Scoglietti[b], and Geof Harston[‡a]
[a]Celight, Inc., 12200 Tech Road, Silver Spring, MD 20904
[b]ITT Corporation, 5901 Indian School Road NE, Albuquerque, NM 87110

ABSTRACT

Progress in standoff detection of surface-bound explosives residue using photothermal and photoacoustic (PT/PA) imaging and spectroscopy has been reported recently. Photothermal/photoacoustic interferometry (PTI), a variation of the aforementioned techniques, is a candidate for standoff detection as a result of its non-contact and non-destructive approach. In PTI, the transient PT/PA hydrodynamic response produced by impulsive infra-red laser excitation(s) are detected by an overlapping focused probe laser beam. The return back-scattered/reflected probe laser beam is collected and coupled into a single-mode optical fiber. The PT/PA-induced perturbation on the return probe laser, in the form of phase or amplitude modulation or both, is extracted interferometrically. The resulting quadrature signals are digitized and processed to recover the minute PT/PA dynamics above background noise. Characteristic spectra for materials can be obtained by quantifying the PT response as a function of excitation(s) wavelength. The CW probe laser, operating in the 1550 nm range, and the constituents of the coherent detection system are commercial off-the-shelf components. A commercially available and continuously tunable quantum cascade laser (QCL) with output pulse energies up to 50 nJ was employed to generate the PT/PA spectra in the 8.8-10.2 μm range. PTI detected absorption spectra were collected for HMX, RDX, and PETN, with the probe laser system positioned 5 meters away from the explosives targets. In addition, PTI measurements of the stimulated Raman (SR) spectra of ammonium nitrate and 2,4,6-trinitrotoluene obtained using a near-IR OPO laser are described. We believe this is the first-ever application of photothermal techniques to the measurement of the SR effect on solid explosive materials at meaningful standoff distances.

Keywords: explosives detection, standoff detection, photothermal interferometry, photoacoustics, spectroscopy, coherent detection, quantum cascade laser, stimulated Raman.

1. INTRODUCTION

The standoff detection of explosives residues on persons and vehicles (PB/VBIED) constitutes a significant technical problem that warrants both intense interest and focus. Recently, a number of photothermal-inspired approaches have demonstrated some capabilities in addressing the threat within the context of approaches that can be safely deployed. In principle, photothermal and photoacoustic (PT/PA) techniques can provide sensitive, selective, non-contact and non-destructive solutions to this problem at meaningful standoff distances [1]. By their very nature the photothermal panoply of techniques derive their benefit from the direct measurement of materials responses to absorbed energy. In the current context, laser sources are used to couple energy into selected vibrational states of explosives compounds. The ensuing molecular relaxations produce measurable density perturbations to the absorbing and proximal volumes which are measured and quantified. Advancements in quantum cascade laser (QCL) technology into wavelength regimes relevant to the vibrational spectroscopy of explosive materials have been leveraged by other groups in the detection of solid surface-attached residues. Recent examples include imaging of thermal emissions [2] and a transmission spectroscopy which employs a novel high-Q quartz tuning fork resonant at the modulation frequency of the QCL [3]. The thermal emission(s) imaging method exploits the radiative relaxation component of photothermal excitation while the latter method, which is tantamount to a 2-way open path total attenuation, utilizes a very sensitive opto-acoustic receiver to detect losses in transmitted light. In both instances reports show significant performance progress with longer detection range, up to 20 m [3], and sensitivity, 100 ng/cm^2 [2], [3].

[*] Present address: P.O. Box 10321, Silver Spring, MD 20914
[†] Present address: Fibertek, Inc., 510 Herndon Parkway, Herndon, VA 20170
[‡] gharston@celight.com; phone: 1-301-625-7000, fax: 1-301-625-7001; www.celight.com

In contrast to the two methods identified above, the photothermal interferometric approach discussed herein probes the real-time *in-situ* hydrodynamic (acoustic and thermal density changes) response to materials excitation. Photothermal/photoacoustic interferometry (PTI) [4] has a well-established history in the peer-reviewed literature [5], [6]. However, despite its unquestionable successes in "laboratory" circumstances, extending PTI to outdoors scenarios at significant distances presents some problems. The imposition of phase and amplitude noise on the sensing (probe) beam by the atmosphere is but one of the problems limiting the application of interferometric techniques in an open and uncontrolled environment. To mitigate the effects of ambient "noise" on PTI measurements a novel coherent receiver system employing advanced noise-cancelation algorithms has been developed. The experimental system construct that enabled collection of the PTI data described below employed this high sensitivity coherent detector to extract phase and amplitude changes imparted to the probe laser specifically by the target materials as a consequence of their relaxations from energy acquired via either direct IR absorption or by a stimulated Raman (SR) process, provoked using a QCL or solid-state OPO laser, respectively.

In the PTI system, pulsed tunable infra-red strobe lasers (QCL or OPO) are used to selectively excite the target explosives molecules. The ensuing hydrodynamic relaxations, whether they take the form of propagating pressure (acoustic mode) or thermal (diffusive mode) waves, result in a time-dependent spatially localized density perturbation that manifests as a change in refractive index which alters the phase/amplitude of the coincident probe beam. The returned (back-scattered/reflected) probe laser beam is collected and the phase and/or amplitude modulation is detected interferometrically. Since the magnitude of the induced phase (amplitude) shift is proportional to the amount of energy absorbed by the material, spectra can be obtained by tuning the strobe lasers through a selected set of frequencies.

Coherent detection of the return probe signal generates a pair of quadrature signals, I and Q. These signals are digitized and processed to recover the small time-dependent phase and amplitude signals that reflect the sample's response to energy acquisition (absorption or Raman) above background noise, producing an absorption (Raman) spectrum of the surface-borne explosive residue. Digital signal processing (DSP) reduces the effects of ambient vibrations and turbulence, improving and extending the range of the pulsed PTI technique, thereby enabling meaningful standoff explosives detection in practical situations.

For this work, excitation of explosives residues was accomplished in two orthogonal spectroscopic modes, namely, stimulated Raman and infra-red absorption. In the case of the stimulated Raman work the entire 6 – 10μm spectral region, known to be highly selective for explosives, was targeted and accessed using a novel NIR-OPO. While for the direct absorption measurements a low duty cycle pulsed QCL tunable over the range from 8.8-10.2 μm was employed.

Five types of solid explosives were investigated: HMX, RDX, PETN, TNT and ammonium nitrate (AN). Direct absorption PTI spectra were collected for HMX, RDX, and PETN which were deposited as films cast from solutions on non-absorbing surfaces. SR PTI spectra were collected for TNT and AN, and likewise rendered from solutions as films on non-absorbing surfaces. In all cases the standoff distance between the receiver and the sample targets was 5m.

2. PHOTOTHERMAL INTERFEROMETRY

2.1 Photothermal Effect

In photothermal interferometry a tunable excitation laser (strobe) illuminates the material of interest. In the general context of a surface-borne IED residue the target material can be comprised of a single, or multiple chemical constituents. Thus, the judicious choice of excitation wavelengths is critical to the success of detecting and identifying these compounds. Towards this end, the excitation wavelengths are selected so as to have maximum transmittance through the atmosphere while retaining maximum selectivity toward the explosives compounds.

Localized explosives' specific excitation is followed by intra (T_1) and intermolecular (T_2) relaxation processes culminating in a propagating acoustic wave (nano/microsecond dynamics) concurrent with a purely dissipative (non-propagating) thermal diffusion (microsecond dynamics) component. Both of these relaxation mechanisms conspire to produce a time-dependent density change with a concomitant experimentally observable change in refractive index. The radiative decay channel is not productive in the context of PTI and will not be discussed here. Additional dynamical complications arise as the absorbing material may transfer both mechanical and thermal (entropy) energy to adjacent materials (both substrate and proximal air mass). The extent to which such energy transfer occurs is manifested in several physical processes that are well-known, and have been investigated [4], [7] and applied in many areas from

spectroscopy, microscopy, imaging, flaw inspection, to material characterization [8], [9], [10], [11]. Some of these energy releasing processes are:

1. Localized temperature increase on the surface.
2. Heat conduction from the heated surface to the surrounding air layer producing a refractive index change in the air column.
3. Thermal piston effect: modulated heat flow from a heated surface into an adjacent air layer, causing thermally modulated expansion and contraction of the air layer over a thickness approximately equal to the thermal diffusion length. The modulated air layer expansion acts as a piston that drives acoustic waves into the air column.
4. Surface thermoelastic expansion: localized surface displacement.
5. Generation of outward propagating surface acoustic Rayleigh wave.
6. Transient surface reflectance change.

The total amount of energy released by the photo-excited molecules is distributed and shared by the above processes (neglecting thermal emission) which may all occur simultaneously, albeit with different time scales. The conversion efficiency of these energy-release processes depends upon many factors related to the morphological, thermochemical, and transport properties of the explosive, substrate, and air mass.

2.2 Excitation Processes

Photoexcitation of the target molecules can be done efficiently through linear processes, such as direct absorption, or non-linearly, for example by a stimulated Raman (SR) process. The rate of linear absorption can be written as

$$R_{lin} = \sigma_{lin} N (P_p / h\nu_p),$$

where σ_{lin} is absorption cross-section at pump frequency ν_p, N is the density of molecules and P_p is the pump laser power density.

Stimulated Raman-induced excitation has been applied to PT/PA spectroscopy previously for both vapor and condensed phases [12], [13], [14]. Stimulated Raman-induced excitation is a 4-wave non-parametric mixing process achieved by overlapping Pump and Stokes laser beams with frequencies ν_p and ν_s on a sample. When the resonance condition,

$$\nu_p - \nu_s = \nu_R,$$

is met, where ν_R is a frequency of a Raman-active mode, the Stokes beam is amplified at the expense of the Pump beam. Each Stokes photon thus generated leaves the molecule with one quantum of excess vibrational energy at ν_R. The subsequent relaxation from an ensemble of such excited molecules releases energy into the surroundings in the various forms described previously. The relaxation dynamics accompanying population of Raman active vibrations are generally not distinguishable from those populated by direct absorption. The rate of stimulated Raman* induced excitation in the incoherent† limit can be written as:

$$R_{Raman} = (d\sigma / d\Omega) (P_s / P_0) N (P_p / h\nu_p),$$

where $(d\sigma / d\Omega)$ is the spontaneous Raman cross-section, P_s and P_p are the Stokes and Pump laser power densities, respectively, and $P_0 = (\Gamma \nu_s) / (\pi \lambda_s^2)$ where Γ is the Raman linewidth which is determined by the pump laser linewidth. As an example, assume $\lambda_s = 2.525$ μm and a Raman linewidth is 1 cm^{-1} i.e. $\Gamma \sim 2\times10^{-23}$ J, yielding $P_0 \sim 0.012$ W/cm^2. Typical values for the spontaneous Raman cross-section of explosives range between 10^{-27}-10^{-31} cm^2. Therefore, for a Stokes laser peak intensity of $P_s > 1.2\times10^6$ W/cm^2, the strength of stimulated Raman excitation can be brought into the same range as linear absorption. Such peak intensities can be readily achieved using nanosecond OPOs to generate

---

* The stimulated Raman effect is a 3rd-order non-linear process requiring spatio-temporal overlap of optical fields and associated matter waves.

† The "incoherent" limit obtains when the rate of Raman excitation is much slower than the rates of dephasing (T_2) processes (collisions, spontaneous emission).

correlated Pump and Stokes fields which, with suitable optics, can be brought to an appropriate focus to meet the radiance requirements for efficient Raman generation.

The motivation for exciting explosives by both direct absorption and SR lies in the fact that the fusion of complimentary spectroscopic data from both Raman and absorption measurements enhances the capability to identify explosive materials.

2.3 Photothermal Interferometry and Coherent Optical Detection

Photothermal Phase Shift

Both the absorption (linear) and the stimulated Raman (non-linear) processes give rise to vibrational excitations of the molecules associated with the explosive compound on the surface. In the absence of any chemistry taking place the ultimate fate of absorbed energy is to produce work and heat. Evidence of mechanical work takes the form of density changes brought on by acoustic waves (fast kinetics) while heat manifests as a combination of density (slow kinetics) changes and thermal emissions. Regardless of the observable being measured, whether it be the time-dependence to the phase of a probe beam in PTI or the emitted radiation, the strength of the measured signal directly correlates to how much energy is partitioned into these decay channels and the amount of energy initially absorbed. For PTI, both the acoustic and the thermal waves produce a time-dependent, localized change in the refractive index resulting in a phase-shift that can be measured using standard interferometric methods.

The refractive index perturbation that is probed by PTI derives from an underlying density change resulting from the absorption of light. In the limit of small acoustic attenuation and thermal time constants it can be shown that the acoustic-limited density perturbation induced by absorption occurs on a time scale approximated as: $t_a = w/c_s$, where, w and c_s are the excitation laser beam radius and the speed of sound, respectively. By contrast, the characteristic time for thermal diffusion induced density perturbations is: $t_c = w^2/4D_T$, with $D_T = \kappa/\rho C_p$, where D_T is the thermal diffusivity, κ the thermal conductivity, and ρC_p the volumetric heat capacity. In the case of explosives materials, sound velocities* of a few thousand m/s are typical. Consequently, typical PTI transients (see Figure 1) exhibit fast acoustic (~100s ns) and slow (acoustic and thermal) components.

To gain further insights into the pulsed photothermal process for an absorbing residue on a spectroscopically innocent (non-absorbing) substrate, approximate expressions for the photothermal phase shift for both direct and stimulated Raman-induced excitation have been derived and are provided below for reference. The temperature rise associated with heating of the illuminated region by a pulsed excitation laser is simply the ratio of the energy density absorbed ΔQ to the heat capacity as follows,

$$\Delta T \approx \Delta Q / \rho C ,$$

where ρC is an effective volumetric heat capacity for the residue. The photothermal induced optical phase shift (double-pass) of the probe beam due to processes associated with heat conduction from the absorbing or excited surface to the surrounding air layer and thermoelastic expansion (ΔL) of the residue can be expressed as [7]

$$\Delta\phi \approx 2\frac{2\pi}{\lambda_{probe}}\ \Delta n_a \mu_a - n_a \Delta L\ \approx 2\frac{2\pi}{\lambda_{probe}}\left[\left(\frac{dn}{dT}\right)_a \Delta T \mu_a - n_a \mu_s \beta_s \Delta T\right]$$

$$\approx 2\frac{2\pi}{\lambda_{probe}}\left[\left(\frac{dn}{dT}\right)_a \mu_a - n_a \mu_s \beta_s\right]\frac{\Delta Q}{\rho C} \approx -2\frac{2\pi}{\lambda_{probe}}\left[\frac{n_a - 1}{T_a}\mu_a + n_a \mu_s \beta_s\right]\frac{\Delta Q}{\rho C},$$

where λ_{probe} is the probe laser wavelength, n_a is the air refractive index, T_a is the equilibrium air temperature, $(dn/dT)_a \approx -(n_a - 1)/T_a$ is the air thermo-optic coefficient, $\mu_{a,s}$ are the air and residue thermal diffusion lengths, respectively, and β_s is the linear thermal expansion coefficient of the residue. Normal incidence of the probe beam to the substrate surface is

* The speed of sound in explosives compounds is in part determined by the crystal's space-group symmetry. In general, there are two transverse (shear) and one longitudinal (compression) modes. For example, for tetragonally symmetric PETN ($P4\bar{2}_1c$ space group) there are 11 unique velocities propagating along the four principal crystal axes. Speeds range from a low of 1300 m/s to high of ~3100 m/s.

assumed. Based on the relatively simple expression above, the photothermal phase shift can be conveniently expressed in terms of measurable quantities such as mass density, laser pulse energy, and the thermodynamic parameters.

For direct absorption, the photothermal phase shift is given by

$$\Delta\phi \approx -2\frac{2\pi}{\lambda_{probe}}\left(\sqrt{\frac{\kappa_a}{\kappa_s}\frac{\rho_s C_s}{\rho_a C_a}}\frac{n_a-1}{T_a}+n_a\beta_s\right)\frac{1}{\rho_s C_s}\frac{N_{Av}}{m_{mol}}\sigma\rho_m N_{layer}\frac{2E_{ex}}{\pi w_{ex}^2},$$

for stimulated Raman-induced absorption, the photothermal phase shift is given by

$$\Delta\phi_R \approx -2\frac{2\pi}{\lambda_{probe}}\left(\sqrt{\frac{\kappa_a}{\kappa_s}\frac{\rho_s C_s}{\rho_a C_a}}\frac{n_a-1}{T_a}+n_a\beta_s\right)\frac{1}{\rho_s C_s}\times$$

$$\left[\frac{2}{\pi}\frac{1}{c^2 h}\frac{1}{n_s^2}\frac{1}{\nu_s^3\nu_p}\frac{\nu_R}{\Delta\nu_R}\frac{N_{Av}}{m_{mol}}N_{layer}\rho_m\frac{1-e^{h\nu_R/k_B T_s}}{1+e^{h\nu_R/k_B T_s}}\frac{d\sigma}{d\Omega}\frac{4\ln 2}{\pi}\frac{4E_p^2}{\pi w_p^2\ \ \pi w_s^2}\frac{1}{\sqrt{t_p^2+t_s^2}}\right].$$

Definitions of the symbols can be found in Table 1 and Table 2.

Table 1. Parameters used for computation of the photothermal phase shift induced by direct absorption for PTI measurements.

PARAMETERS	***SYMBOL***
Probe laser wavelength	λ_{probe}
Strobe laser focused beam radius at the target	w_{ex}
Strobe laser pulse energy	E_{ex}
Refractive index of air	n_a
Equilibrium air temperature	T_a
Thermal conductivity of air	κ_a
Volumetric heat capacity of air	$\rho_a C_a$
Thermal conductivity of surface residue	κ_s
Volumetric heat capacity of surface residue	$\rho_s C_s$
Linear thermal expansion coefficient of surface residue	β_s
Number of explosive residue monolayers	N_{layer}
Avogadro's number	N_{Av}
Molar mass of compound, (g/mole)	m_{mol}

Table 2. Parameters used for computation of the photothermal phase shift induced by stimulated Raman excitation for PTI measurement. Other parameters not listed here can be found in Table 1.

PARAMETERS	***VALUES***
Pump laser wavelength or wavenumber	λ_p , ν_p
Stokes laser wavelength or wavenumber	λ_s , ν_s
Refractive index of surface at λ_s	n_s
Focused Pump beam radius at the target	w_p
Focused Stokes beam radius at the target	w_s
Pump laser pulse energy	E_p
Stokes laser pulse energy	$(\nu_s / \nu_p)\, E_p$
Pump laser pulse width (FWHM)	t_p
Stokes laser pulse width (FWHM)	t_s
Raman transition wavelength or wavenumber	λ_R , ν_R
Raman transition linewidth	$\Delta\nu_R$
Equilibrium surface temperature	T_s
Boltzmann constant	k_B

PTI system

PTI uses a probe laser beam to sense and an analyzer to detect and quantify interferometrically, in a manner similar to a coherent LADAR, the photothermal phase and amplitude shifts.

As described previously, pulsed and wavelength tunable strobe lasers excite the target molecules inducing the transient change in the refractive index of the target and surrounding materials (mostly air). The relaxation processes in the photo-excited molecules produce two temporally distinguishable density-change phenomena in the medium proximal to the excited molecules: a fast acoustic wave transient followed by a slower thermal recovery to thermal equilibrium. These phenomena are observable by changes in the refractive index and are sensed via an induced phase change imparted to the non-absorbed probe beam, Figure 1. The phase changes in the probe are quantified and directly related to the concentration of the energy-absorbing chemical by the analyzer subsystem. The magnitude of the phase shift correlates to the optical absorption (linear dependence on laser power), or stimulated Raman (bilinear laser power dependence) characteristics of the material; by tuning the strobe to a number of laser lines PTI detected spectra* result.

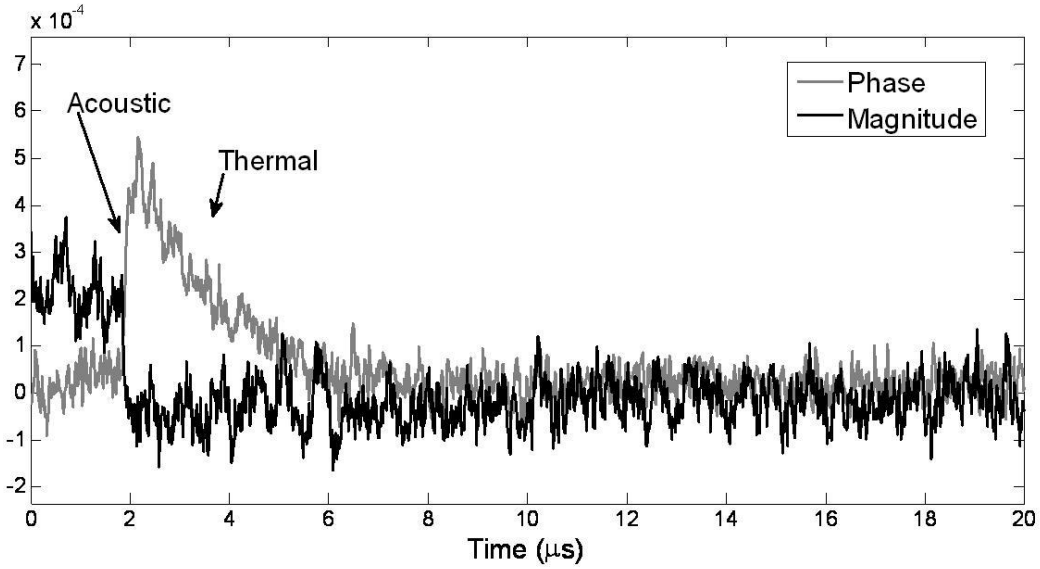

Figure 1. Phase and magnitude components of the photothermal transient. The fast acoustic wave and the slow thermal recovery of the relaxation dynamics can both be seen. The data shown is for a TNT film on gold mirror with NIR excitation.

The strob*e* laser subsystem constitutes the wavelength tunable excitation source in the PTI system. For operation in the acoustic limit the strobe laser's pulse length satisfies $\tau_{laser} << t_a$. A judicious selection of excitation (strobe) laser lines enables PTI measurements to be more selective and sensitive towards the chemicals of interest despite the presence of complex backgrounds and interferents. For SR excitation, two strobe beams, Pump and Stokes, whose difference can be tuned resonantly to the target's vibrations are required.

The probe laser beam is aligned to be spatially coincident with the strobe excitation laser pulses at the target surface. The selection of an optimal probe wavelength is based on considerations of atmospheric transmittance, and the availability of high-power laser sources and interferometric components that can be operated in field conditions and achieve a maximum SNR. The probe laser can be operated near 1550 nm or any other convenient wavelength.

* PTI spectra more accurately reflect the true nature of matter-materials interactions compared to optical transmission techniques as PTI is sensitive ONLY to perturbations due to energy acquired by the material under test. Elastic scattering, which plagues optical measurements on solid materials, does not impact PTI.

The analyzer is a digital coherent pulsed interferometer that is capable of extracting the signal-derived phase change from air-turbulence, target movement, and vibration. The analyzer is composed of a local laser oscillator, a coherent receiver, and a digital signal processing unit with embedded DSP algorithms.

A portion of the phase-shifted return probe beam is collected and coupled into the coherent receiver for homodyne balanced detection, which allows measurement of both the phase and magnitude of the optical signal. The receiver is comprised of a quadrature optical hybrid [15], in which the signal and the local oscillator are mixed, and a pair of balanced photoreceivers.

The optical hybrid is a six port device that mixes a signal, the returned probe beam in this case, and a reference to produce four outputs; denoting the complex input optical fields of the returned probe and reference beams by S and R, the four outputs of an ideal optical 90° hybrid are simply, $S \pm R$ and $S \pm jR$. The four outputs are coupled into a pair of balanced photoreceivers in such a way as to produce the in-phase and quadrature-phase components (I and Q) of the signal. The voltage outputs of ideal balanced photoreceivers with conversion gain G (V/W) are: $A\cos(\varphi_s+\varphi_n)$ and $A\sin(\varphi_s+\varphi_n)$ where $A=G|S||R|$. The PT/PA-induced phase shift and the background phase noise are denoted by φ_s and φ_n respectively.

Some of the advantages of coherent detection are that the received signal is boosted by the local oscillator for shot-noise limited receiver sensitivity and linear down-conversion of the received signal to the electrical baseband, which enables adaptive DSP-based noise reduction algorithms, including phase noise induced by physical phenomena such as mechanical vibrations, Doppler shift, and air turbulence.

The SNR for shot-noise limited homodyne balanced detection expressed in terms of the photothermal phase shift $\Delta\varphi$ is given by,

$$\mathrm{SNR} \approx \frac{2\eta P_{rec}}{h\nu_{probe} B} \Delta\phi^2 ,$$

where $h\nu_{probe}$ is the probe laser photon energy, η is the quantum efficiency of the detector, P_{rec} is the average optical power of the received probe laser, and B is the receiver noise bandwidth. The optical field of the returned probe laser collected by the receiver can be expressed as,

$$[\, S(t) + n(t) \,] \cdot e^{j[\varphi_s(t) + \varphi_n(t)]},$$

where $S(t)$ and $\varphi_s(t)$ are, respectively, the optical amplitude and phase generated by the photothermal phenomenon and $n(t)$ and $\varphi_n(t)$ are background noise. The optical field amplitude modulation $S(t)$ can be caused by a surface reflectance change, beam defocusing, or beam deflection initiated by the photothermal effect. The single-pass phase shift signal $\varphi_s(t)$ can be caused by a path length change: $\varphi_s(t) = 2\pi n_a \Delta L(t)/\lambda_{probe}$ where $\Delta L(t)$ can be caused by localized surface displacement or surface acoustic Rayleigh wave [16], [17]. $\varphi_s(t)$ can also be produced by a photothermal refractive index change $\Delta n(t)$ over an effective distance L in an air column above the surface giving $\varphi_s(t) = 2\pi\Delta n(t)L/\lambda_{probe}$. Effective background noise suppression can be achieved by observing that the energy releasing processes are much faster than $n(t)$ and $\varphi_n(t)$ so that the noise is essentially frozen in time compared with $S(t)$ and $\varphi_s(t)$. Despite this tolerance to relative low-frequency noise, a wideband photodetector is required to preserve the temporal fidelity of $S(t)$ and $\varphi_s(t)$.

The I and Q electrical signals from the coherent detector are digitized and DSP methods, based on adaptive algorithms and Kalman prediction techniques, are used to further improve the SNR. The background noise in the I and Q signals of the PTI waveform is very high compared with the acoustic transient of the PTI signal. This noise is attributed to airflow across the probe laser beam path, environmental acoustic noise such as cooling fans, mechanical vibrations (low frequencies), and electromagnetic radiation picked up by the detection electronics (high frequencies). However, by observing the fast micro-second acoustic transient, the measurement is essentially immune to this low-frequency (~ kHz) noise (see section 4.3).

3. MEASUREMENT SETUP

The PTI system was comprised of three sub-systems: the strobe, the probe, and the coherent analyzer. A schematic of the PTI system is shown in Figure 2.

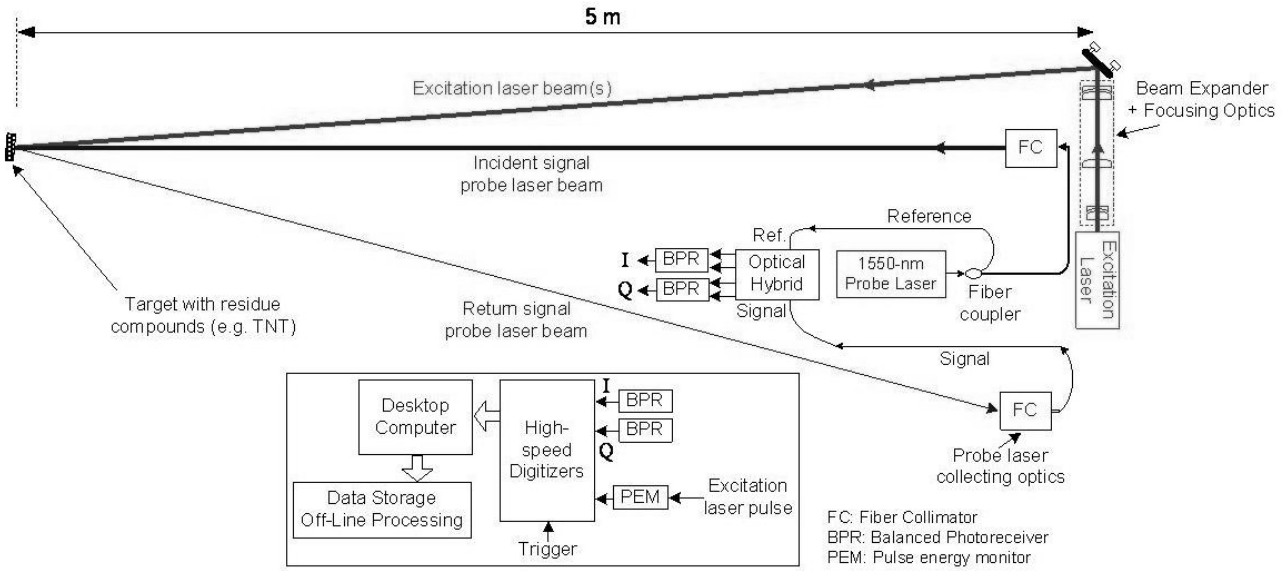

Figure 2. Schematic of the standoff PTI test system.

3.1 Strobe

The strobe sub-system was comprised of the tunable, pulsed, excitation laser (either OPO or QCL), and the beam expanding and focusing optics. A mirror is used to steer the strobe beam to overlap the probe at the target.

Quantum Cascade Laser

The excitation laser for the direct absorption measurements was a commercially available QCL from Daylight Solutions. The QCL was tunable over the 8.8-10.2 μm wavelength range and was set to generate output pulses with widths of 500 ns and energies up to 50 nJ at a 100 kilo-pulses per second repetition rate.

In a variation from Figure 2 the QCL was placed ~0.5 m from the target due to the availability of optics for the beam expanding and focusing. We believe that the results are still applicable to longer standoff distances due to the negligible atmospheric absorption over the wavelength range.

Optical Parametric Oscillator

The stimulated Raman excitation was implemented by spatially and temporally overlapping two simultaneously generated near-IR (NIR) photons produced by an Optical Parametric Oscillator (OPO) laser at the surface residue target. The OPO consisted of a set of optics and crystals to create pairs of wavelengths with the Pump wavelength between 1.80 and 1.93 μm and the Stokes wavelength between 2.60 and 2.38 μm. All Raman-active normal modes in the 6 –10 μm region can be accessed by using specific combinations of these tunable NIR wavelengths.

The OPO generated output pulses with widths of 10 ns and energies up to 200 μJ at a 1 kilo-pulses per second repetition rate. The Pump and Stokes beams were directed so that they were co-propagating as they exited the laser. Special care was taken in the design of the beam expanding and focusing optics to insure proper focusing of both beams. As shown in Figure 2, the OPO was 5 m from the target.

3.2 Probe

Similar to the strobe sub-system, the probe sub-system consisted of the probe laser and the focusing optics. Unlike the strobe laser, there are no special spectroscopic requirements for the probe laser. However, in order to maximize the detection sensitivity performance and the SNR the probe laser should meet several criteria. The main requirements of the probe laser are low phase noise (narrow linewidth), frequency stable, good atmospheric transmission, meet eye/skin safety requirements, compatible with the analyzer subsystem (optical hybrids and balanced photoreceivers), and readily available as a commercial off-the-shelf item. The telecom-type 1.55-μm lasers, for example, are good candidates and

there are a variety of commercially available narrow linewidth lasers with good frequency stability, such as fiber lasers, and optical amplifiers for the 1.55 μm wavelength.

A fiber laser operating at ~ 1547 nm and output coupled to a single-mode optical fiber was used as the probe source. The output from the probe laser was divided into two paths via a fiber-optic coupler with a coupling ratio of 99/1. One output of the coupler was directed to an adjustable fiber-collimator (1-inch aperture) in which the probe beam is launched into free-space and focused on the target. The second output of the coupler was a reference signal, the local oscillator, connected directly to the coherent receiver via optical fiber. The probe laser and the focusing optics were located 5 m from the target as can be seen in Figure 2.

A fiber-collimator similar to the one used in the transmitter was used to collect and couple the reflected/back-scattered probe beam into a single-mode optical fiber.

3.3 Coherent Analyzer

The coherent analyzer was comprised of the coherent receiver, consisting of an optical 90° hybrid followed by a pair of balanced photoreceivers (BPR), high speed analog-to-digital convertors (ADCs), and a computer, serving as the data storage and digital signal processing unit.

The collected reflected/back-scattered probe beam and the reference, coupled off of the probe laser, were directed to the two inputs of the optical 90° hybrid and the hybrid outputs are coupled into the balanced photoreceivers. The two resulting electrical signals were digitized using a pair of ADCs at 100 MS/s and stored for off-line processing. Up to 1s of the signal was captured and stored. A TTL trigger signal that was synchronized with the strobe pulse was also captured and provided a window indicating when the PT/PA perturbation occurred. The captured data was analyzed to extract the PT/PA-induced phase shift for different strobe wavelengths. The extracted phase shift was assumed to be proportional to the absorbance and the laser pulse energy.

3.4 Target Materials and Substrate

The target consisted of each explosive deposited on a protected gold mirror (1-inch diameter). PTI data taken of the gold mirrors showed them to be spectroscopically innocent over the strobe wavelength ranges. Relatively high average mass densities of the explosive materials were used for these initial measurements. Table 3 gives the average mass densities for each measurement.

Table 3. Mass densities of the explosive materials used in each measurement.

Material	***Excitation Source***	***Average Mass Density (mg/cm^2)***
HMX	*QCL*	26.5
RDX	*QCL*	8.1
PETN	*QCL*	15
TNT	*OPO (SR)*	30
AN	*OPO (SR)*	55
TNT	*OPO (Stokes beam only)*	1.4

4. MEASUREMENT RESULTS

The calculated spectra from the PTI measurements are shown in the figures below. In each PTI experiment one measurement was taken without the strobe beam applied to the target in order to obtain the system background; this background measurement is included in the figures. Also included in the figures are "reference" spectra obtained on the same samples from either Fourier transform infrared (FTIR) or FT-Raman measurements.

4.1 PTI Measurement with Direct Absorption

In general, the 19-line PTI acquired spectra (Figures 3 – 5) show good agreement with the FTIR spectra despite the low per pulse energies of the QCL source. While differences between the PTI and FTIR spectra were not unexpected, as FTIR measures light attenuation which includes elastic scattering loses, the difference between the two in the PETN case

stands out given the similarities in the HMX and RDX spectra; the difference may be due to contamination, deterioration, weak absorption, or residue-substrate interfacial interactions. What is indisputable from these data is the fact that in the absence of interferents these spectra are of sufficient quality to enable unambiguous identifications of the three explosives to be made. In particular, the two nitramines, RDX and HMX, are readily distinguishable on the basis of these spectra.

In addition to the explosives materials, a painted portion of a car body was measured in anticipation of the deposition of explosives samples on legitimate backgrounds such as car panels for the assessment of standoff detection of VBIEDs by PTI. Multilayer vehicle coatings pose a potential interference problem owing to overlapping infra-red absorption features coming from the protective topcoat and pigment-bearing basecoat sublayers. A relatively strong, albeit unstructured spectrum (Figure 6) is observed for the car panel. Despite this strong background absorption explosive residues can be easily detected by exploiting differences in the PT kinetics between explosives and vehicle coatings (data not shown).

On the basis of the success of these measurements, it is anticipated that similar results will be obtained throughout the LWIR as QCLs are now available that continuously span the entire 6 – 10μm wavelength range.

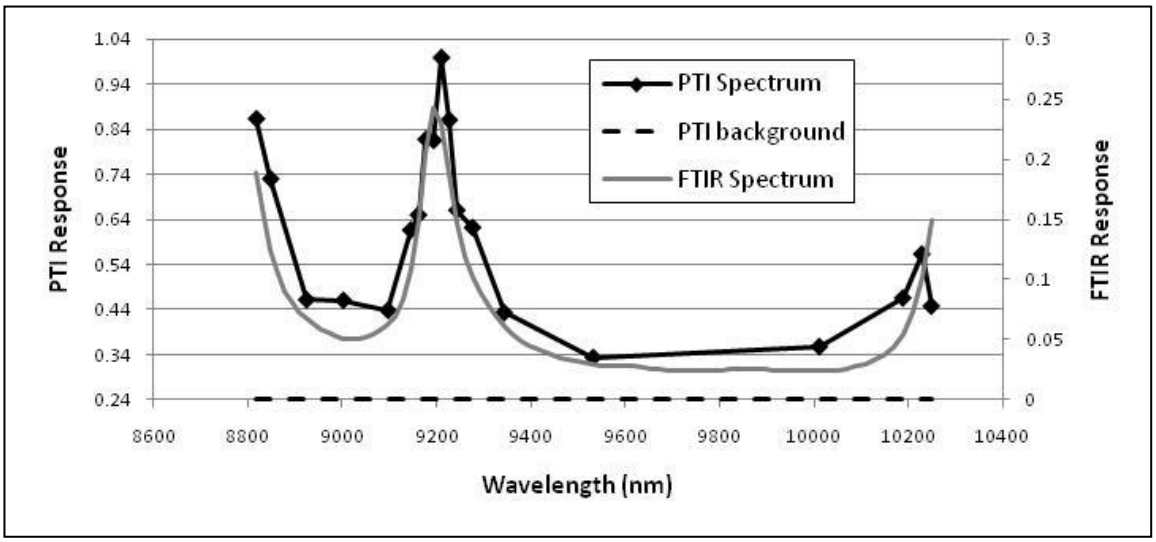

Figure 3. Comparison of PTI and FTIR absorption spectra of HMX.

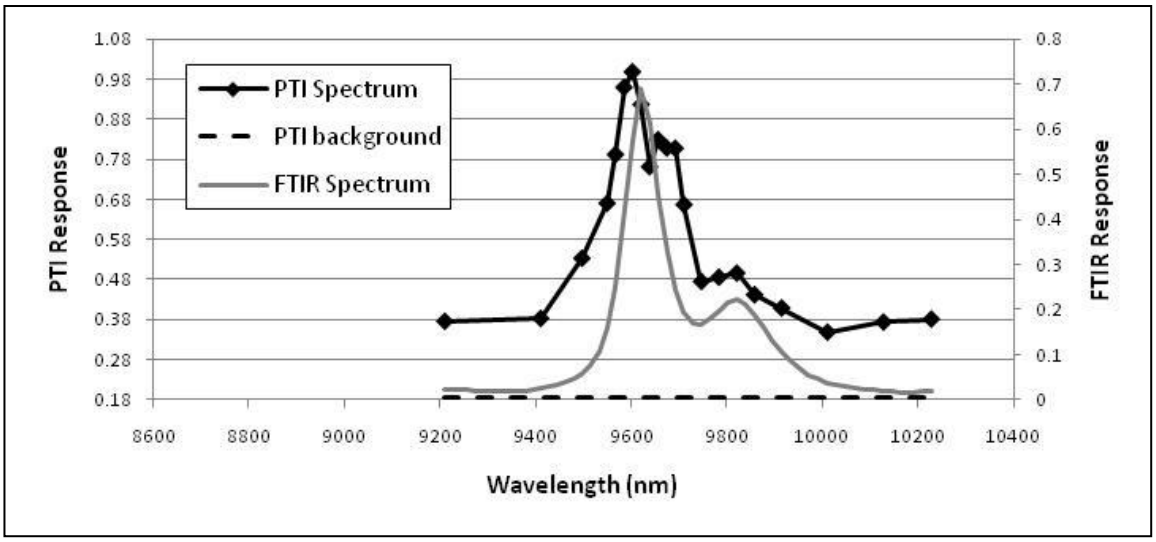

Figure 4. Comparison of PTI and FTIR absorption spectra of RDX.

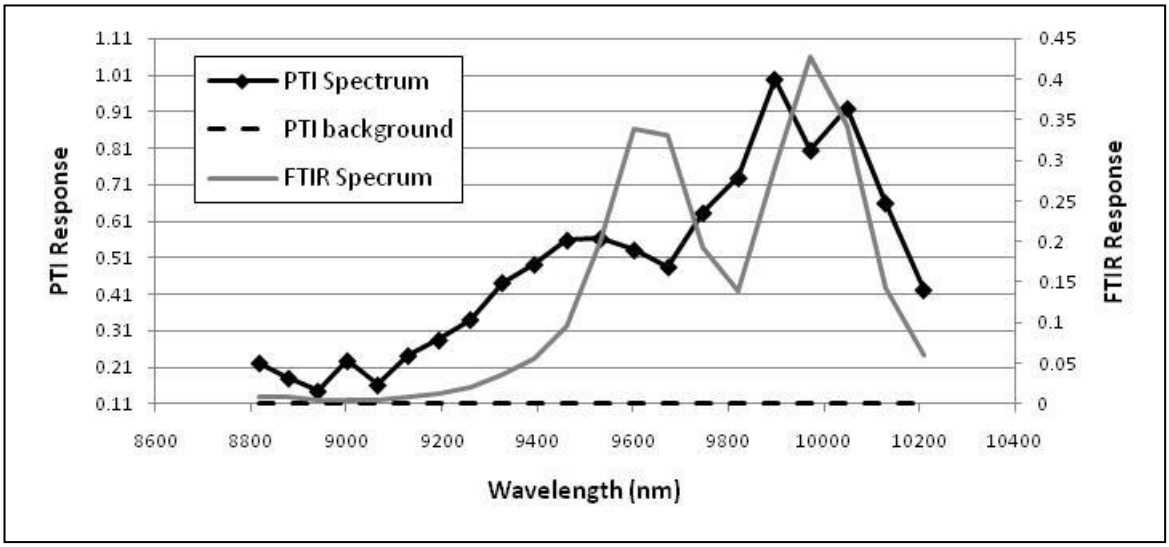

Figure 5. Comparison of PTI and FTIR absorption spectra of PETN.

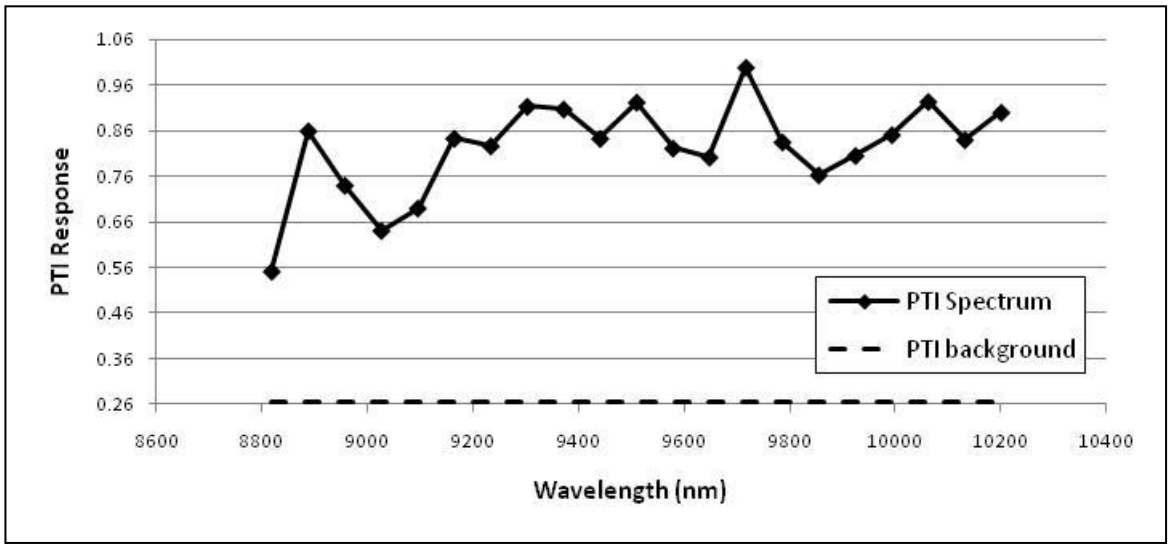

Figure 6. PTI absorption spectrum of a car body (FTIR spectrum not shown).

4.2 PTI Measurements made with Stimulated Raman Excitation

In order to access the spectroscopically significant 6- 8 μm range, acknowledged to be highly selective for N-containing explosives, while maintaining the applicability of PTI detection a stimulated Raman approach was evaluated. While QCL lasers spanning the 6-8μm wavelength range are available, attenuation from atmospheric water vapor in this region precludes propagation of many valuable wavelengths at meaningful standoff distances. In order to circumvent this atmosphere problem a tunable NIR-OPO was employed to selectively excite Raman-active resonances for TNT (Figure 7) and ammonium nitrate (Figure 8). The spatiotemporal coincidence of the signal and idler components of the OPO at range were confirmed through a sum frequency generation process in an appropriate non-linear crystal. The PTI

measured 8-line stimulated Raman* spectra show excellent congruence to the FT-Raman spectra for both materials. In the absence of interferents these spectra are of sufficient quality to enable unambiguous identifications of the two explosives.

These data indicate that PTI has the requisite sensitivity to produce useful spectra generated by a 3rd-order non-linear process.

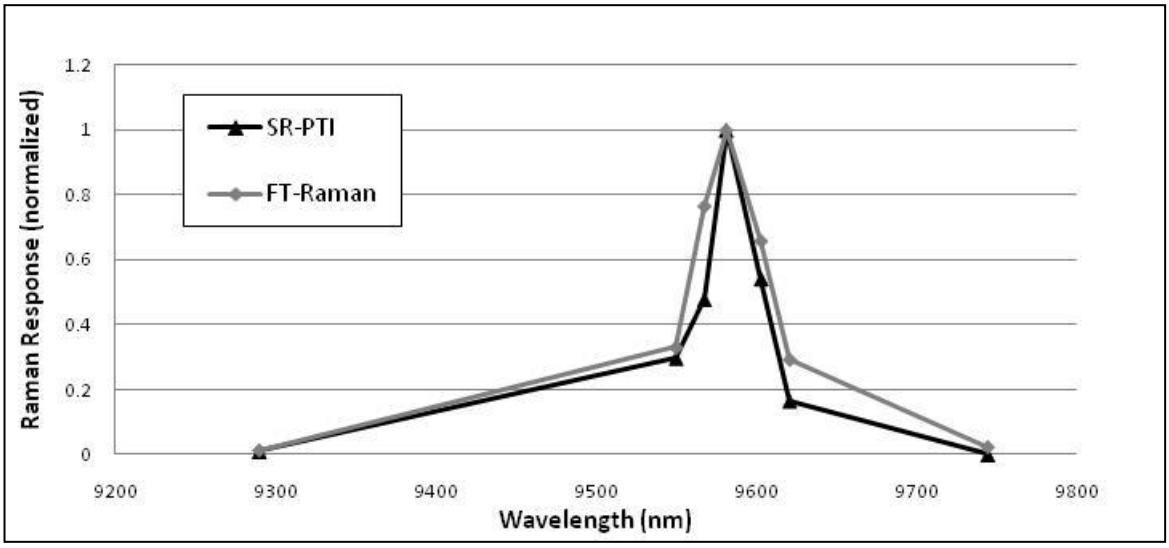

Figure 7. Comparison of PTI and FT-Raman spectra of AN. The spectrum is of the symmetric stretch of the NO_3^- ion which is forbidden by IR selection rules but Raman allowed.

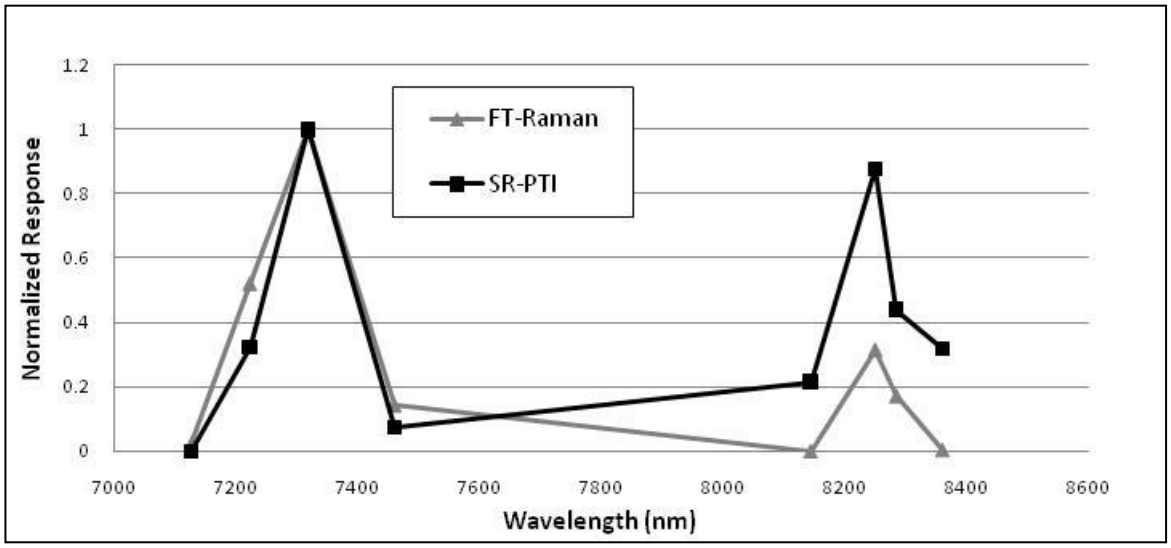

Figure 8. Comparison of PTI and FT-Raman spectra of TNT.

* In the incoherent limit, the stimulated Raman process is directly proportional to the spontaneous Raman cross-section. The stimulated Raman spectrum should look like the spontaneous spectrum.

4.3 Turbulent Transmission Path

Air turbulence is a major source of phase and amplitude noise that can have a negative impact on PTI measurements. As a test of the ability of the PTI DSP algorithms to mitigate the effects of air induced noise, NIR-PTI measurements of TNT residues were taken under conditions where turbulent air was deliberately introduced along the transmission path of the strobe/probe lasers. The turbulence was generated by a 1500W electric space heater placed half way (~2.5 m) down the transmission path blowing directly at the beam paths. Two temperature settings were used to generate relative "low" and "high" air turbulence. The target was a thin film of TNT on a gold mirror with mass density of approximately 1mg/cm^2 positioned at 5m distance from the experimental system.

Figure 9 shows the decreasing signal-to-background ratios of the measured PTI spectra as the level of turbulence increases. This diminishing SBR is not due to a reduction in the transient phase shift but to fading in the received probe signal. Figure 10 shows the same data after normalization showing that the turbulence induced "noise" has been successfully cancelled resulting in TNT spectra that are indistinguishable from one another and in excellent agreement with the FTIR spectrum. Consequently, DSP retrieval algorithms preserve the spectral fidelity of the PTI signals under conditions that induce significant phase an amplitude noise. It is expected that similar successes would be obtained in more general circumstances where the combined effects of air turbulence, target vibration, and ambient acoustics are present.

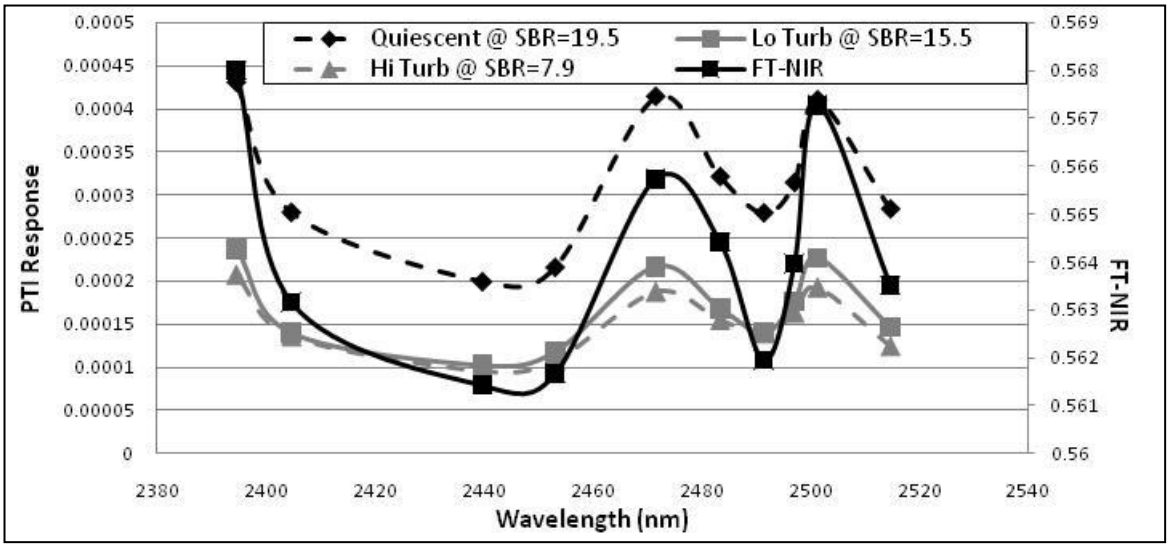

Figure 9. Comparison of PTI and FTIR absorption spectra of TNT for various levels of air turbulence.

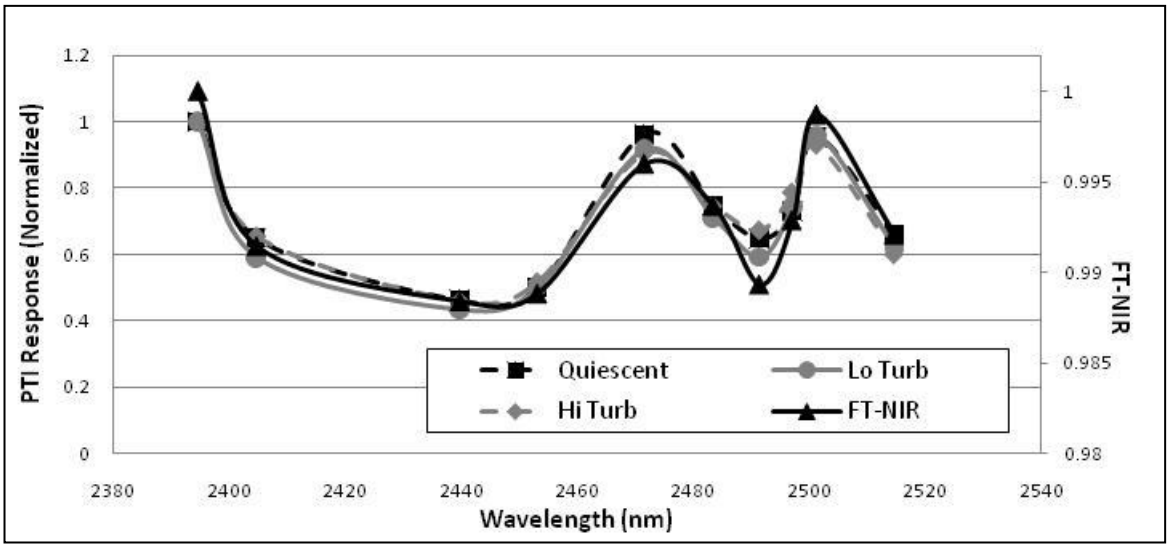

Figure 10. Comparison of Normalized PTI and FTIR absorption spectra of TNT for various levels of air turbulence.

5. CONCLUSION

The use of the novel coherent receiver system, which employs high-speed sampling of the acoustic transient and advanced noise-canceling algorithms, enables the use of photothermal interferometry in open and uncontrolled environments, allowing PTI to be used for meaningful standoff detection of surface-bound explosives residues. Even in turbulent environments with significant background noise imparted to the probe signal, accurate PTI spectra can be measured.

Recent developments in quantum cascade lasers now provide access to the highly spectroscopically informative LWIR range. Continuously tunable QCLs spanning the spectral range of 6 – 12μm are available. Using a broadly tunable pulsed QCL(s) with a maximum average power, at 5% duty cycle, of ~4.5 mW standoff detection of explosives (HMX, RDX, PETN) with a PTI system has been shown. Much higher power QCL sources are becoming commercially available. This suggests the possibility of using QCLs as the excitation source for PTI measurements in PB/VBIED applications.

Alternatively, stimulated Raman induced excitation using a novel short-pulse tunable NIR-OPO which exploits available atmospheric transmission windows has also been shown as a viable method of achieving photothermal excitation for PTI measurements of explosives specific Raman resonances in the LWIR. This method allows continuous access to regions of the LWIR that are generally unavailable to direct laser propagation as a result of high atmospheric absorption. *It is expected that the fusion of data from two complimentary spectroscopic probes, direct absorption and Raman, will enable enhanced capability to identify threats including explosives.*

ACKNOWLEDGMENTS

The authors would like to thank Daylight Solutions for providing the tunable QCL used in this work. This research was supported in part through ITT Internal Research and Development projects.

REFERENCES

[1] Skvortsov, L. A., Maksimov, E. M., "Application of laser photothermal spectroscopy for standoff detection of trace explosive residues on surfaces," Quantum Electronics 40(7), 565-578 (2010).

[2] Papantonakis, M. R., Kendziora, C., Furstenberg, R., Stepnowski, S. V., Rake, M., Stepnowski, J., and McGill, R. A., "Stand-off detection of trace explosives by infrared photothermal imaging," Proc. of SPIE 7304, 730418 (2009).

[3] Van Neste, C. W., Senesac, L. R., and Thundat, T., "Standoff spectroscopy of surface adsorbed chemicals," Analytical Chemistry 81(5), 1952-1956 (2009).
[4] Bialkowski, S. E., [Photothermal Spectroscopy Methods for Chemical Analysis], John Wiley & Sons, Inc., (1996).
[5] Davis, C. C., and Petuchowski, S. J., "Phase fluctuation optical heterodyne spectroscopy of gases," Applied Optics 20(14), 2539-2554 (1981).
[6] Davis, C. C., "Trace detection in gases using phase fluctuation optical heterodyne spectroscopy," Appl. Phys. Lett. 36(7), 515-518 (1980).
[7] Tam, A. C., "Applications of photoacoustic sensing techniques," Reviews of Modern Physics 58, 381 (1986).
[8] Harris, M., Pearson, G. N., Willets, D. V., Ridley, K., Tapster, P. R. and Perrett, B., "Pulsed indirect photoacoustic spectroscopy: application to remote detection of condensed phase," Appl. Opt. 36, 1841 (2000).
[9] He, Q., Vyas, R. and Gupta, R., "Theory of photothermal spectroscopy in an optically dense fluid," Appl. Opt. 36, 1841 (1997).
[10] Hutchins, D. A., and Tam, A. C., "Pulsed photoacoustic materials characterization," IEEE Trans. Ultrasonics, Ferroelectrics, and Frequency Control 33, 429 (1986).
[11] Cooper, J. A., Crosbie, R. A., Dewhurst, R. J., Mckie, A. D. W. and Palmer, S. B., "Surface acoustic wave interactions with cracks and slots: a noncontacting study using lasers," IEEE Trans. Ultrasonics, Ferroelectrics, and Frequency Control 33, 462 (1986).
[12] Barrett, J. J. and Berry, M. J., "Photoacoustic Raman spectroscopy (PARS) using CW laser sources," Appl. Phys. Lett. 34, 144 (1979).
[13] West, G. A., Siebert, D. R. and Barrett, J. J. "Gas phase photoacoustic Raman spectroscopy using pulsed laser excitation," J. Appl. Phys. 51, 2823 (1980).
[14] Patel, C. K. N. and Tam, A. C., "Optoacoustic Raman gain spectroscopy of liquids," Appl. Phys. Lett. 34, 760 (1979).
[15] Kaplan, A., Achiam, K., Greenblatt, A., Harston, G. and Cho, P. S., "LiNbO3 Integrated Optical QPSK Modulator and Coherent Receiver," ECIO Conference Proc., 79-82 (2003).
[16] Nadeau, F. and Hutchins, D. A., "A study of the interaction of surface waves with slots using non-contact laser generation and detection of ultrasound," IEEE Ultrasonics Symp. Proc., 921 (1984).
[17] Sugawara, Y., Wright, O. B., Matsuda, O., Takigahira, M., Tanaka, Y., Tamura, S. and Gusev, V. E., "Watching ripples on crystals," Phys. Rev. Letts. 88, 185504-1 (2002).